Katzengold R, Orlov A, Gefen A.
A novel system for dynamic stretching of cell cultures reveals the mechanobiology for delivering better negative pressure wound therapy.
Biomech Model Mechanobiol. 2020 Aug 14.
doi: 10.1007/s10237-020-01377-6.

Ms. Ref. No. **BMMB-D-20-00156 (Revision)** July 22nd, 2020

A novel system for dynamic stretching of cell cultures reveals the mechanobiology for delivering better negative pressure wound therapy

Rona Katzengold, Alexey Orlov, Amit Gefen*

Department of Biomedical Engineering, Faculty of Engineering, Tel Aviv University, Israel

***Corresponding author:**

Amit Gefen, Ph.D.
Professor of Biomedical Engineering
The Herbert J. Berman Chair in Vascular Bioengineering
Department of Biomedical Engineering
Faculty of Engineering
Tel Aviv University
Tel Aviv 6997801
Israel
Tel. +972-3-6408093
Fax. +972-3-6405845
E-mail: gefen@tauex.tau.ac.il

Keywords

Chronic and acute wound healing; scratch wound assay; cell biomechanics; surgical wounds; tissue repair

Submitted to *Biomechanics and Modeling in Mechanobiology*

Abstract

Serious wounds, both chronic and acute (e.g. surgical) are among the most common, expensive and difficult to treat health problems. Negative pressure wound therapy (NPWT) is considered a mainstream procedure for treating both wound types. Soft tissue deformation stimuli are the crux of NPWT, enhancing cell proliferation and migration from peri-wound tissues which contributes to healing. We developed a dynamic stretching device (DSD) contained in a miniature incubator for applying controlled deformations to fibroblast wound assays. Prior to the stretching experiments, fibroblasts were seeded in 6-well culture plates with elastic substrata and let to reach confluency. Squashing damage was then induced at the culture centers and the DSD was activated to deliver stretching regimes that represented common clinical NPWT protocols at two peak strain levels, 0.5% and 3%. Analyses of the normalized maximal migration rate (MMR) data for the collective cell movement revealed that for the 3%-strain level, the normalized MMR of cultures subjected to a 0.1Hz stretch frequency regime was ~1.4-times and statistically significantly greater (p<0.05) than that of the cultures subjected to no-stretch (control) or to static stretch (2nd control). Correspondingly, analysis of the time to gap closure data indicated that the closure time of the wound assays subjected to the 0.1Hz regime was ~30% shorter than that of the cultures subjected to the control regimes (p<0.05). Other simulated NPWT protocols did not emerge as superior to the controls. The present method and system are a powerful platform for further revealing the mechanobiology of NPWT and for improving this technology.

1. Introduction

Serious wounds, both chronic and acute, are among the most common, expensive and difficult to treat health problems. A recent study evaluated that such wounds impact nearly 15% of the US Medicare beneficiaries and are associated with a conservative estimated expenditure of $32 billion, and up to $97 billion when considering costs associated with infections (Nussbaum et al. 2018). The most expensive treatment cost estimates were for surgical wounds, followed by diabetic foot ulcers and pressure ulcers (Padula and Delarmente 2019).

During the proliferative phase of the normal wound healing cascade, dermal fibroblasts proliferate and migrate into the wound bed to fill the gap, synthesize growth factors and produce new extracellular matrix (ECM). This fibroblast migration results in the expression of thick actin bundles that form scar tissue (Stroncek and Reichert 2008; Singer and Clark 1999). As such, fibroblast migration into wounds is vital for healing and therefore, *in vitro* "wound healing" assays typically focus on the kinematics of migration of these cells, e.g. through transwell assays, stopper-based assays and scratch assays (Rodriguez-Menocal et al. 2012; Lin et al. 2019; Fronza et al. 2009; Walter et al. 2010). The cell migration behavior observed in monolayer fibroblast culture models *in vitro* was found to be informative and useful with respect to understanding *in vivo* cell migration, specifically with regards to factors that accelerate or inhibit collective fibroblast migration, including mechanobiological factors (Pijuan et al. 2018; Trepat et al. 2012; Liang et al. 2007; Monsuur et al. 2016; Pinto et al. 2019).

Mechanical deformations and stresses are naturally applied to human wound sites by bodyweight forces, physiological function (e.g. respiratory movements acting

on a sternal wound after cardiac surgery) and application of treatment dressings. In addition, in many cases, loads are delivered to the wound bed as part of a treatment plan, via negative pressure wound therapy (NPWT). Use of NPWT grew exponentially since the 1990's and it is now considered a mainstream procedure for treating both surgical and chronic wounds (Apelquist et al. 2017; Yadav et al. 2017; Othman 2012). In NPWT, vacuum is locally applied to the wound site, inducing drainage of the wound bed and thereby reduction of the edema concurrently with micro- and macro-deformations of the wound and peri-wound tissues, which mechanically stimulate cells to proliferate and migrate (Vikatmaa et al. 2008; Huang et al. 2014; Apelqvist et al. 2017; Lalezari et al., 2017). The mechanisms of action of NPWT are not completely understood to date, particularly with regards to the cell-scale effects (Lalezari et al., 2017). This is manifested in a large variety of modes of operation of the commercially available NPWT devices, the alternative NPWT protocols, programed options and adjustable parameters that are set in practice, primarily based on clinical judgement and experience. Cells in the soft tissues subjected to NPWT may therefore be exposed to highly variable mechanical stimuli, depending on the specifications of the device in use, the chosen device settings, clinical protocols and the mechanical properties of the peri-wound/wound tissues of the individual.

It is well known that micro- and macro-scale mechanical deformations applied to cells influence fundamental cellular functions and biological processes, including morphological features, the likelihood of proliferation, rate of differentiation, adhesive interactions, apoptosis and in the context of the present work, the speed and directionality of collective cell migration (Paluch et al. 2015; van Helvert et al. 2018). Numerous experimental reports demonstrated that the mechanical stretching of cells

triggers intracellular biochemical signaling which increases the expression of various proteins e.g. fibronectin, alters gene expression and activates molecular pathways of proliferation, differentiation or angiogenesis (Tokuyama et al. 2015; Huang et al. 2014; Pandit et al. 2015; Ao et al. 2015; Lalezari et al., 2017). Specifically, it has been shown that fibroblasts (Marom et al. 2019), adipocytes (Shoham et al. 2012), myoblasts (Nagai et al. 2012), vascular endothelial cells (Naruse et al. 1998), chondrocytes (Hirano et al. 2008) and bronchial fibroblasts (Kato et al. 1998) respond to stretching stimulations by modulating cell shapes and cytoplasmic organization where typically, cytoskeleton fibers form, orient and resist the shape changes by the mechanical forces (Chanet and Martin 2014; Undyala et al. 2008; Angelini et al. 2010). It is therefore not surprising that collective migration patterns and speeds are affected by stretching of the cell substrata. Our group statically stretched scratch-wound fibroblast assays to evaluate how stretching of the cultures influences migration rates (Toume et al. 2017). We reported that exposing these scratch assays to static 3% strain increased the normalized migration rates and reduced the gap closure time relative to unstretched controls or exposure to a 6% strain level (Toume et al. 2017). Our other published work further indicated that exposure to 9% strain or higher strain levels led to plasma membrane poration followed by apoptotic cell death (Slomka and Gefen 2012).

Our published research (Toume et al. 2017) and the work of others clearly indicated that micro-deformations of the wound bed and peri-wound tissues are beneficial for wound healing in the specific aspect of accelerating fibroblast migration (Wiegand and White 2013). Fibroblasts subjected to certain small strain regimes migrate to longer distances (Chow et al. 2016) or faster (Toume et al. 2017), however, the optimal strain values and cycle frequencies remain unknown. Accordingly, while

NPWT systems clearly deliver good clinical outcomes, their design, programming and adjustments are decided much like a shot in the dark, as no relevant mechanobiological knowledge exists to guide industry work in this regard. Deeper understanding of the mechanobiology of NPWT will pave the way for a better-informed device design process and thereby, improved wound care technologies which optimize the stimuli to the wound site for a faster tissue repair. This paper describes a fundamental and vital step in this direction. First, a novel method and system have been developed to determine the collective fibroblast migration kinematics under dynamic stimuli used in NPWT. Second, the present work utilized the above new experimental system for comparing common clinical NPWT protocols, translated to the mechanobiological environment of cultured fibroblasts, in an effort to identify a preferred cell stimulation regime that accelerates the collective migration of these cells to their target.

2. Methods

We developed an apparatus - the miniature incubator for cell stretching (MICS) - for applying controlled deformations to wound assays over periods of hours, days or weeks. This apparatus is composed primarily of an incubation chamber and a computer-controlled dynamic stretching device (DSD).

2.1 Cell culturing

NIH3T3 fibroblast cells were maintained in a culture medium composed of Dulbecco's modified Eagle's medium (DMEM) supplemented with 10% fetal bovine serum (FBS), 2mM L-glutamine, 0.1% penicillin/streptomycin (all components of the culture medium were purchased from Biological Industries Co., Israel). Cells were first thawed from liquid nitrogen storage and cultured in 75 cm^2 filter cap flasks for 3 days in an incubator at 37ºC and 5% CO_2. Cells were then passaged by washing the

cultures twice with PBS, applying 1 ml trypsin (0.25%/0.25%) for 5 min, adding 5 ml of culture medium, centrifuging and removing the supernatant. Cells were continuously passaged every 3/4 days and then similarly cultured in 75 cm^2 filter cap flasks. Prior to all cell stretching experiments, cells were seeded in six-well culture plates with elastic, transparent and collagen-coated substrata (BioFlex®, Flexcell International Corporations, Burlington, NC, USA), and were then cultured for 1-2 days until reaching 100% confluency.

2.2 The Miniature Incubator for Cell Stretching

We selected to load the fibroblasts in dynamic stretching modes representing commonly accepted clinical NPWT treatment protocols. Our MICS system was built accordingly, for applying dynamic equibiaxial and homogeneous tensile strains to the cell culture substrata (**Fig. 1**). The current MICS design is based on a previously reported static cell stretching device developed and used by our group in multiple experimental mechanobiological studies (Levy et al. 2012; Shoham et al. 2012; Leopold and Gefen 2013; Slomka and Gefen 2012; Toume et al. 2017), however, the basic design has been substantially improved here, to facilitate the NPWT-like dynamic stretches and the live imaging of the assays.

Specifically, our DSD apparatus contains a geared direct current (DC) step motor (IDEA driver, Haydon kerk, AMETEK) that is placed on the superior bridge and rotates a screw which elevates and lowers the inferior bridge. The inferior bridge is connected to rods which press over the flexible bottoms of the culture plate, which is mounted between the two frames of the apparatus. The descent of the superior bridge lowers the plate bottoms over Teflon rings which are 20mm in diameter and that are positioned underneath the culture plate. This thereby stretches the elastic

substrata that make the bottoms of the culture plate (**Fig. 1a,b**). The Teflon rings are hollow at their center, for two main reasons: (i) The light source of the microscopy system is located inferior to the rings, so hollow rings facilitate illumination of the cultures from below, which allows the digital time-series photography of gap closure processes. (ii) It would have been extremely challenging, from a manufacturing perspective, to produce solid posts which are ideally horizontal and smooth across their entire contact surface with the elastic substrata, so that the strain field is not interrupted by irregularities or bumps in the superior surfaces of such posts. We further verified that the elastic substrata used for the cell culturing in the 6-well BioFlex® culture plates (Flexcell® Int. Corp., Burlington NC, USA) and for the further migration studies produce a homogeneous, equibiaxial strain field and also, behave linearly-elastically. This has been accomplished by means of experimental and finite element (FE) methods, as reported in detail in our previously published work (Shoham et al. 2012; Katzengold et al., 2015). In brief, the equibiaxial strain field on the substrata has been characterized using a speckle-tracking-based strain measurement method (Shoham et al. 2012) and the negligibility of edge effects has been demonstrated using FE analyses of the cell stretching system (Katzengold et al., 2015). We further verified the linear-elasticity of the material of the substrata for cell culturing using uniaxial tensile tests, where we have stretched three specimens of the substrata (each being 14 cm long × 2 cm wide) at a rate of 5 mm/min (Instron 5544 model, High Wycombe, UK). The substrata demonstrated a linear-elastic behavior up to a strain magnitude of 18%. Finally, as a safety measure, to avoid any potential edge effects that may influence the equibiaxial strain fields in the culture wells, all the micro-gaps in cultures were created at the approximate centers of the cultures.

This DSD apparatus was carefully designed, in terms of its overall size and material components, to allow it to function continuously in an incubator at 90% humidity, 5% CO_2, and 37°C. The dimensions of the DSD apparatus were 13.5×16×13 cm. The bottom frame of the DSD was made of polycarbonate, and the other parts were made of Stainless Steel 303. The whole apparatus is sterilizable using 70% ethanol (Bio-Lab Ltd., Jerusalem, Israel) before culturing.

We verified and characterized the homogeneous and biaxial strain state in the substrata of the culture plates as follows. When the elastic substrata were in an undeformed configuration, we acquired high-resolution (12.2 megapixel) photographs of three dot-shaped dye marks that were carefully made on the substrata. Then, the top frame was lowered to a defined distance (d) in the motor software and the marks where photographed again in the deformed configuration. These images were processed by a MATLAB code (MathWorks, Natick, MA, USA), and the three Eulerian strain components (E_{cc}, E_{rr}, and E_{rc}) were calculated for each d using the finite strain theory, as detailed in our previously published work (Geddes et al. 2001; Be'ery-Lipperman and Gefen 2005; Lee et al. 1996). The two normal strain components, E_{cc} and E_{rr}, are the strains along the circumferential and radial axes, respectively, whereas E_{rc} is the shear strain component. We calculated these stain components for d in the range of 0.3–1.8 mm which is allowed by the apparatus. We repeated this calibration experiment three times for each well and for three wells (i.e. 9 repetitions) and calculated the mean strains. For an ideal equibiaxial strain, $E_{cc} = E_{rr}$ and $E_{rc}= 0$ (Lee et al. 1996) and hence, the mean tensile strain E was calculated as the average of E_{cc} and E_{rr}. We fitted the plot of E versus d with a linear function (with a Pearson correlation coefficient= 0.969) (**Fig. 2**):

$$E = 69d/10000 \qquad (1)$$

where *d* in the above equation is provided in units of millimeters. To fit the stretching apparatus properly above the objective of the microscope, a custom-designed stage was 3D-printed. In addition, the condenser was raised using 2 custom designed rods and a condenser connecting plate, using the same screw connections of the original microscopic stage.

Cell viability was maintained throughout the experiments using a custom-made transparent incubation chamber made of Perspex, with wall thickness of 10 mm which contained the entire microscope setup but allowed for manual refocusing of the microscope if needed, during the experiments. The temperature within the incubation chamber was maintained at 37˚ using a heater mat and rod (model 245-635, RS Components Co., Corby, United Kingdom) and a thermocouple (621-2164, RS Components Co., Corby, United Kingdom) which were connected to a temperature controller PXR4 (Fuji, 539-5101 RS Components Co., Corby, United Kingdom). A DC brushless fan (YM1208PTS1, Huaxia Hengtai, Longhua District, Shenzhen, China) was included in the incubation chamber design for temperature homogeneity and circulation, which prevent focus shifting of the microscope. The pH was further kept nearly constant, at a level of 7.6, by adding 0.5% of HEPES to the culture media. To maintain a steady CO_2 level in the incubation chamber, an Okolab Airpump and CO_2 tank were connected to a CO2 - O2 manual gas mixer (2GFmixer, Okolab, NA, Italy) and an outflow of 1 nl/min air and 0.05 ml/min CO2 was installed. A tent structure build from a squared silicone mat (250x300mm) was squeezed around the condenser of the microscope and further fixed around the microscopic stage to maintain the CO_2 and humidification in the proximity of the cells (**Fig. 1c**).

2.3 Experimental design

To inflict cell damage, the confluent monolayers were mechanically squashed using the sharp point of a needle which was centered by a custom 3D-printed cross handle (**Fig. 3a**). Using the above needle, a quasi-static load was applied to create an approximately circular 'wound' gap in the culture well of interest. After puncture, cells were washed with 2 ml PBS to remove the debris of the dead cells prior to investigation of the damaged culture. Next, 5 ml of culture medium were added and the culture plate was placed in the MICS apparatus, which was subsequently placed on the custom microscopy stage.

Damaged cultures were stretched using two peak strain levels, 0.5% and 3%, which are equivalent to negative pressures of approximately 75 and 200 mmHg, respectively (Katzengold et al. 2018). The experiments where a 0.5% peak strain level was used included the following stretch protocols: (i) No stretch (which served as controls), (ii) static stretch ('ramp-and-hold', as a second control group), (iii) 1 Hz cycles (representing an intermittent NPWT wave form), (iv) 0.1 Hz cycles (representing a slower intermittent wave form); and (v) cycles of 5 minutes of continuous stretch followed by 2 minutes of a relaxation period (often referred to in the wound care literature as a '2-5' protocol, which is another form of an intermittent NPWT wave). The cyclic as well as the '2-5' NPWT protocols are commonly used in clinical practice (Dastouri et al., 2011; Hong, 2013; Lee et al. 2015, Apelqvist et al. 2017). The experiments where a 3% peak strain has been set were conducted similarly, using the above stretch protocol types, excluding the 1 Hz cycles which were too rapid for the MICS hardware to adequately deliver the stretches from a system control perspective (**Fig. 3b**).

2.4 Time-lapse imaging

A digital inverted phase contrast microscope (Nikon Eclipse TS100) with a Nikon CFI Achro DL objective using 10×magnification, a working distance of 7 mm, and numerical aperture of 0.25 acquired the culture images. Culture photographs were taken every 5 minutes until the gap completely closed, by means of a Nikon DS-Fi1 digital camera with resolution of 2560×1920 pixels. Before image data were analyzed we have omitted the specific images taken while the gap was stretched, and only used the images acquired at a relaxed substrate state, since the gap changes its size cyclically during stretching, whereas we were interested in isolating the parameters of gap closure by the collective cell migration.

2.5 Analysis of gap closure

In order to analyze the time-progression images of the gap closure and further quantify the collective cell migration into the formed gaps, we used a MATLAB code that was developed in our group for this purpose and employed widely in our published work (Topman et al. 2012a,b & 2013a; Monsuur et al. 2016). Briefly, the gap area is quantified automatically by applying a custom-made image processing algorithm (Fig. **4a**) which segments each analyzed micrograph (at each time point in the acquired sequence) into two regions: a denuded region versus a cell-populated (surrounding) region. This segmentation is done based on local image texture properties: the denuded region is characterized by a more homogeneous image texture (variability of pixel intensities in a region of interest) than the cell-populated region. The above image processing algorithm was applied to each individual frame along the time sequence, and for every experiment, to ultimately produce a gap area (A) over time (t) plot, per each trial. These A–t plots were then fitted to a Gaussian function and the maximal slope of the fitted curve has been reported here as the normalized

MMR. The normalized root-mean-square error of the fit was always less than 5% and typically (for 95% of data points) lower than 1%, which indicates an adequate and robust fitting procedure.

2.6 Statistical testing

We conducted at least 5 repetitions for each experimental protocol used in our 0.5%-strain stretching studies, and also, at least 10 repetitions of the 3%-strain studies. We then compared the mean of the kinematic parameters (e.g. the normalized MMR and time for 90% 'wound' closure) using one-way analysis of variance (ANOVA), per each peak strain level, to determine whether the stretching protocol caused a statistically significant difference in cell migration response to the infliction of damage in the cultures. Since the 3%-strain data indicated significant differences, we further conducted post-hoc pairwise Tukey-Kramer tests to identify the specific differences between each pair of protocol types. A *p*-value lower than 0.05 was considered statistically significant.

3. Results

Every *A*-*t* plot of all the wound assays always exhibited a sigmoidal behavior with the steepest downward slope, i.e. the normalized MMR occurring within the 2nd to 3rd quartiles of the total closure period, which was 5-14 hours for the pooled data from all the stretching protocols (**Fig. 4**). Analyses of the normalized MMR data (**Fig. 5a,b**) further revealed that for the 3%-strain level, the normalized MMR of fibroblast cultures subjected to the 0.1 Hz regime was ~1.4-times and statistically significantly greater (p<0.05) from that of cells subjected to no-stretch (control) or to static stretch (2nd control). Nonetheless, the 2-5 stretching protocol was statistically indistinguishable from the two aforementioned controls (**Fig. 5a**). In addition and correspondingly, analysis of the time to gap closure (coverage of 90% of the gap area)

data (**Fig. 5c,d**) indicated that the closure time of the wound assays subjected to the 0.1 Hz regime was ~30% lower than that of the cultures subjected to the control regimes (p<0.05). The same assays conducted at 0.5%-strain peaks resulted in similar ranges of normalized MMR and closure time data with respect to the 3%-peak datasets (normalized MMR: 19.8-27.9 %-area/hr; time to 90% gap closure: 5.2-8.6 hours) but the results of the 0.5%-strain dataset were statistically indistinguishable across the different stretch protocols. This observation appeared to be associated with an overall substantially greater variability in the kinematic data of the tested cultures for the 0.5%-strain experiments with respect to the data from the 3%-strain cultures (**Fig. 5b,d**).

4. Discussion

NPWT is one of the most important non-pharmaceutical platform technologies developed and applied for tissue repair and wound healing. A key feature of NPWT is that it maintains the environment of the wound-bed as a semi-isolated compartment, which facilitates control over the applied biomechanical stimuli, leading to beneficial cell-scale biological effects that macroscopically enhance the wound healing process (Apelquist et al. 2017; Yadav et al. 2017; Othman 2012). Mechanical deformations of the wound-bed and peri-wound tissues are the crux of NPWT. These mechanical stimuli are considered to enhance tissue perfusion, vascular and lymphatic vessel growth, migration and proliferation of immune and tissue-repairing cells, as well as differentiation of epithelial cells (Lee et al. 2015; Huang et al. 2014; Pandit et al. 2015; Ghazanfari et al. 2009). All the above lead to epithelization of the wound-bed, granulation, revascularization and eventually, to tissue repair and scar formation (Singer and Clark 1999).

We developed a novel experimental mechanobiological model system which enables real-time, live-imaging of collective cell migration in response to inflicted localized damage in the studied cultures. In the present work, we employed this model system for experimentally evaluating the influence of specific and commonly used deformation regimes on *en mass* migration of fibroblasts, towards development of improved NPWT technologies and protocols for treating acute and chronic wounds. The above model system builds up on a decade of mechanobiological work in our research group in the field of wound healing, including the live-imaging and image processing methods and algorithms employed here (Topman et al. 2012a,b & 2013a; Monsuur et al., 2016). Our published contributions have revealed fundamental kinematic characteristics of collective cell migration, including the sigmoidal nature of the area-versus-time curves reported in the works of Topman et al. (2012a,b), a phenomenon which is consistently demonstrated here again (**Fig. 4a-e**).

One NPWT protocol studied here, which is often used when treating chronic wounds such as pressure ulcers/injuries and diabetic foot ulcers, is five minutes of negative pressure followed by two minutes of relaxation (Lee et al. 2015; Apelqvist et al. 2017). In our present study, we simulated the effect of this protocol on collective migration in fibroblast cultures subjected to localized mechanical damage (by cyclically applying 5 minutes of static stretch to the cultures with an induced gap, in a ramp-and-hold manner, followed by two minutes of relief). Interestingly, we found that this 2-5 regime was inferior, in terms of the resulting migration kinematics, with respect to a more frequent, 0.1 Hz stimulus (having the same 3%-strain peak). Specifically, the 0.1 Hz stimulus was associated with a 18%-greater normalized MMR (**Fig. 5a**) and a 12%-lower coverage time (**Fig. 5c**) compared with the 2-5 regime. In fact, while the 2-5 regime data were statistically indistinguishable from the ‘no-

stretch' and 'static-stretch' control experiments, the 0.1 Hz regime was statistically significantly different with respect to both of these control types, with greater migration speeds and shorter closure times as reported in the Results section. This is a seminal discovery, as it is the first time in the literature where a laboratory methodology has been developed in order to mechanobiologically evaluate and compare between NPWT protocols. Moreover, the new MICS system was able to identify a preferable NPWT protocol in the aspect of the collective cell migration kinematics.

Another vital observation made in the present study is that the amplitude of the stretching stimuli is a critically important parameter. For the 3%-strain levels we note that the 0.1 Hz regime resulted in statistically significantly greater normalized MMRs and shorter closure times than for the controls (and the 2-5 regime), however, these kinematic results were substantially more variable and therefore non-significant for the 0.5%-strain datasets. In this context, the literature indicates that collective migration of gastric mucosal cells cyclically stretched to strains of 5–10% (i.e. larger strains than those used in our work) was slower than that of non-stretched cultures, likely due to disruptions to cytoskeletal structures and cell adhesions (Osada et al. 1999). Similar results were reported for exposure of airway epithelial cells to 20%-strain peaks (Desai et al. 2010). In contrast, when studying lower-level dynamic stretches, our group (Toume et al. 2016) demonstrated that a strain range of 3-6% did not alter the cytoskeleton or increased the cell death rates. Here, we further showed that 0.5%-strain peaks are a sub-optimal stimulus, and so, while not damaging the cells (based on our previous work; Toume et al., 2016), they do not have a positive effect on migration either. We therefore conclude that, not surprisingly, Goldilocks principle applies in the context of the mechanobiology of NPWT: To enhance

collective migration, peak strains delivered to cells and tissues need to be not too little, nor too high.

The limitations of the present MICS system and the experiments reported here primarily concern the study of monolayers of cells, which does not consider the complex three-dimensional (3D) cell organization in tissue structures, as well as the related interactions of cells with the extracellular matrix (ECM). While we have studied cell migration in 3D tissue-engineered hydrogel-based constructs before (Topman et al. 2013b), in our experience, the elegance of a monolayer system allows for effective and robust extraction of the parameters of the migration kinematics; the ECM structure and composition would add another layer of complexity, particularly in the context of wounds where the ECM is partially or fully degraded. The presently described method and system allow, in effect, for high-throughput studies of NPWT protocols in interaction with other cell therapies such as pharmaceutical and natural medications which are used or considered for use in wound healing (Topman et al. 2013a). This will be our next research goal. Another limitation which should be considered here, is that we did not isolate effects of cell proliferation or non-specific cell death and how these could potentially be influenced by the different stretching protocols. Within the 14-hour timeframe of our experiments, migratory activity (and not proliferation) was the paramount contributor to cell coverage of the gaps, as evident from our present video analyses, as well as from our previously published work (Topman et al., 2012b). With that said, in future work, we plan to add a new image processing module for identifications of mitotic and non-specific cell death events (the development of which is already underway in our group; Shkolyar et al., 2015), which would then facilitate determination of the effects that each stretching protocol has on mitosis and non-specific cell death.

The edge of the needle in our setup for inflicting mechanical damage to the studied cell cultures was approximately 250 micrometers in diameter, which theoretically indicates that the damage area within cultures would be approximately 0.05mm^2, however, in practice, deflection of the elastic substrate at the instance of contact with the needle causes a larger damage area, up to 0.09mm^2 (examples of initial gap sizes are provided in **Figure 4**, for the zero time points). This occurs because cells are also irreversibly damaged around the tip of the needle (e.g. due to shear), not just under its compressing edge. The damage area than typically continues to grow, by up to 20% within the first hour post infliction of the mechanical damage (**Fig. 4**). In our earlier published work, we have explained that this is likely due to some short-term apoptosis, as well as that the cells located in proximity to the boundaries of the damage area lose their adhesion to the surface, but not to their neighboring cells. As the neighboring cells exert pulling forces, the cells at the boundaries mildly retreat, which results in the transient increase of the gap area (Topman et al., 2012a). Gap closure commences at approximately 0.5 to 1 hour following the damage infliction, and progresses into full coverage within 5 to 14 hours for the above selected needle size. Importantly, the present damage infliction method was aimed at simulations of deformation-induced death of a relatively small group of cells in a microscopic, early stage of formation of a pressure ulcer or a diabetic ulcer. This is the triggering, cell-scale damage event that may later evolve into a clinically significant chronic wound, according to contemporary etiological descriptions (Gefen, 2019a,b; Gefen et al., 2020). Since the spread area of a single NIH3T3 fibroblast is ~600 μm^2 (Rajagopalan et al., 2004; Topman et al., 2011), our experimental data (**Fig. 4**) indicates that between ~50 and ~150 cells have died directly due to the applied localized mechanical load at the time of the damage

infliction event. These cell numbers were considered sufficient to represent groups of cells dying instantaneously and together, in one location, in order to simulate the microscopic onset of a chronic injury and in particular, the early 'deformation-inflicted' damage phase in the injury cascade which occurs at the microscale of tissues (Gefen, 2019a,b; Gefen et al., 2020).

In summary, by means of our novel MICS setup, we demonstrated that a 0.1 Hz cyclic stretching regime with non-damaging 3%-strain peaks accelerated the collective migration rates of fibroblasts, and more so than the common 2-5 NPWT protocol, indicating that there is benefit in the shorter-cycle recurring mechanical stimuli. The ability to obtain this important information using our MICS system makes the present method and system a powerful platform for further revealing the mechanobiology of NPWT and for improving this technology. In particular, the mechanobiological data produced through our MICS experiments clearly inform the development of better NPWT devices and protocols. This will optimize the delivered cell-level stimuli for achieving faster tissue repair, possibly even adjusting these stimuli to the individual physiology and healing capacity in the future.

To conclude, this is the first study ever to connect between clinical NPWT protocols and quantitative (automated, standardized) analyses of experimental collective cell migration performance data, which facilitates objective comparisons of NPWT protocols in this central mechanobiological aspect. Our present work further demonstrated, for the first time in the literature, that the amplitude and frequency of delivering the dynamic strain loading have fundamental influence on the collective migration behavior of cultured fibroblasts, which could explain why some clinically used NPWT protocols may be more effective than others. Moreover, our work has

demonstrated that a (fibroblast) cell sensitivity threshold of the amplitude of the peak strain stimuli induced by NPWT systems exists. Hence, NPWT systems, NPWT programming or pressure settings which deliver strains lower than that threshold to any tissue regions (e.g. peri-wound tissues) would be ineffective at these tissue sites from a cell migratory perspective. This paves the way for better computational modelling (finite element) studies that map the decay of strain magnitudes from the center of a wound through peri-wound tissues, for evaluating the efficacy of existing or future NPWT systems, as conceptualized in our published work (Katzengold et al., 2018). We have further described a novel method and system for live cell imaging of collective cell migration during dynamic stretching of the studied cultures, which is difficult to achieve from an experimental design perspective. Moreover, the present version of our DSD system is versatile and can be used for testing existing and future NPWT protocols for their impact on collective cell migration, including in interaction with pharmaceutical agents that may affect cell proliferation or migration, or other, biophysical methods which potentially accelerate directional cell migration such as induction of electrical fields (Tai et al., 2018).

Acknowledgements

We would like to thank Mr. Jelle van Orsouw from Eindhoven University of Technology and Dr. Uri Zaretsky from our Department of Biomedical Engineering at Tel Aviv University for their help regarding the development of the cell stretching apparatus and experimental work**.** This research work was partially supported by the Israel Science Foundation grant no. 1266/16 and by the European Union's Horizon

2020 research and innovation programme under the Marie Skłodowska-Curie grant agreement no. 811965.

5. References

Angelini TE, Hannezo E, Trepat X, Fredberg JJ, Weitz DA (2010) Cell migration driven by cooperative substrate deformation patterns. Phys Rev Lett 104:168104.

Ao M, Brewer BM, Yang L, Franco Coronel OE, Hayward SW, Webb DJ, Li D (2015) Stretching fibroblasts remodels fibronectin and alters cancer cell migration. Sci Rep 9;5:8334.

Apelqvist J, Willy C, Fagerdahl AM et al. (2017) Negative Pressure Wound Therapy – overview, challenges and perspectives. J Wound Care 26: 3, Suppl 3, S1–S113.

Be'ery-Lipperman M, Gefen A (2005) Contribution of muscular weakness to osteoporosis: computational and animal models. Clin Biomech (Bristol, Avon) 20(9):984-97.

Chanet S, Martin AC (2014) Mechanical force sensing in tissues. Prog Mol Biol Transl Sci 126:317-352.

Chow SE, Chen CP, Hsu CC, Tsai WC, Wang JS, Hsu NC (2016) Quantifying cell behaviors in negative-pressure induced monolayer cell movement. Biomed J 39(1):50-9.

Dastouri P, Helm DL, Scherer SS, Pietramaggiori G, Younan G, Orgill DP (2011) Waveform modulation of negative-pressure wound therapy in the murine model. Plast Reconstr Surg. 127(4):1460-6.

Desai LP, White SR, Waters CM (2010) Cyclic mechanical stretch decreases cell migration by inhibiting phosphatidylinositol 3-kinase- and focal adhesion kinasemediated JNK1 activation. J Biol Chem 285, 4511–4519.

Fronza M, Heinzmann B, Hamburger M, Laufer S, Merfort I (2009) Determination of the wound healing effect of Calendula extracts using the scratch assay with 3T3 fibroblasts. J Ethnopharmacol 126(3):463-7.

Geddes DM, Cargill RS 2nd (2001) An in vitro model of neural trauma: device characterization and calcium response to mechanical stretch. J Biomech Eng. 123(3):247-55.

Gefen A, Alves P, Ciprandi G, et al (2020) Device-related pressure ulcers: SECURE prevention. J Wound Care. 29(Sup2a):S1-S52.

Gefen A, Brienza D, Edsberg L, Milton W, Murphy C, Oomens CWJ, Perry L, Sari Y. (2019a) The etiology of pressure injuries. In: Prevention and Treatment of Pressure Ulcers/Injuries: Clinical Practice Guideline European Pressure Ulcer Advisory Panel (EPUAP), National Pressure Injury Advisory Panel (NPIAP) and the Pan Pacific Pressure Injury Alliance (PPPIA), 3rd Edition.

Gefen A (2019b) How medical engineering has changed our understanding of chronic wounds and future prospects. Med Eng Phys. 72:13-18.

Ghazanfari S, Tafazzoli-Shadpour M, Shokrgozar MA (2009) Effects of cyclic stretch on proliferation of mesenchymal stem cells and their differentiation to smooth muscle cells. Biochem Biophys Res Commun 388(3):601-5.

Hirano Y, Ishiguro N, Sokabe M, Takigawa M, Naruse K (2008) Effects of tensile and compressive strains on response of a chondrocytic cell line embedded in type I collagen gel. J Biotechnol 133:245–52.

Hong JP (2013) Addressing the vertical and horizontal aspects of the wound by using negative pressure wound therapy and growth factors. Wounds International 4(4):6-7.

Huang C, Leavitt T, Bayer LR, Orgill DP (2014) Effect of negative pressure wound therapy on wound healing. Curr Probl Surg 51:301–31.

Kato T, Ishiguro N, Iwata H, Kojima T, Ito T, Naruse K (1998) Up-regulation of COX2 expression by uni-axial cyclic stretch in human lung fibroblast cells. Biochem Biophys Res Commun 244:615–9.

Katzengold R, Shoham N, Benayahu D, Gefen A (2015) Simulating single cell experiments in mechanical testing of adipocytes. Biomech Model Mechanobiol. 14(3):537-47.

Katzengold R, Topaz M, Gefen A (2018) Dynamic computational simulations for evaluating tissue loads applied by regulated negative pressure-assisted wound therapy (RNPT) system for treating large wounds. J Tissue Viability. 27(2):101-13.

Lalezari S, Lee CJ, Borovikova AA, Banyard DA, Paydar KZ, Wirth GA, Widgerow AD (2017) Deconstructing negative pressure wound therapy. Int Wound J. 14(4):649-57.

Lee AA, Delhaas T, Waldman LK, MacKenna DA, Villarreal FJ, McCulloch AD (1996) An equibiaxial strain system for cultured cells. Am J Physiol 271(4 Pt 1):C1400-8.

Lee KN, Ben-Nakhi M, Park EJ, Hong JP (2015) Cyclic negative pressure wound therapy: an alternative mode to intermittent system. Int Wound J 12(6):686-92.

Leopold E, Gefen A (2013) Changes in permeability of the plasma membrane of myoblasts to fluorescent dyes with different molecular masses under sustained uniaxial stretching. Med Eng Phys. 35(5):601-607.

Levy A, Enzer S, Shoham N, Zaretsky U, Gefen A (2012) Large, but not small sustained tensile strains stimulate adipogenesis in culture. Ann Biomed Eng 40(5):1052-60.

Liang CC, Park AY, Guan JL (2007) In vitro scratch assay: a convenient and inexpensive method for analysis of cell migration in vitro. Nat Protoc 2(2):329-33.

Lin JY, Lo KY, Sun YS (2019) Effects of Substrate-Coating Materials on the Wound-Healing Process. Materials (Basel) 12(17):2775.

Marom A, Berkovitch Y, Toume S, Alvarez-Elizondo MB, Weihs D (2019) Non-damaging stretching combined with sodium pyruvate supplement accelerate migration of fibroblasts and myoblasts during gap closure. Clin Biomech (Bristol, Avon) 62:96-103.

Monsuur HN, Boink MA, Weijers EM, Roffel S, Breetveld M, Gefen A, van den Broek LJ, Gibbs S (2016) Methods to study differences in cell mobility during skin wound healing in vitro. J Biomech 49(8):1381-1387.

Nagai Y, Yokoi H, Kaihara K, Naruse K (2012) The mechanical stimulation of cells in 3D culture within a self-assembling peptide hydrogel. Biomaterials 33:1044–51.

Naruse K, Yamada T, Sokabe M (1998) Involvement of SA channels in orienting response of cultured endothelial cells to cyclic stretch. Am J Physiol 274(5 pt 2):H1532–8.

Nussbaum SR, Carter MJ, Fife CE, DaVanzo J, Haught R, Nusgart M, Cartwright D (2018) An Economic Evaluation of the Impact, Cost, and Medicare Policy Implications of Chronic Nonhealing Wounds. Value Health 21(1):27-32.

Osada T, Watanabe S, Tanaka H, Hirose M, Miyazaki A, Sato N (1999) Effect of mechanical strain on gastric cellular migration and proliferation during mucosal healing: role of Rho dependent and Rac dependent cytoskeletal reorganisation. Gut 45, 508–515.

Othman D (2012) Negative pressure wound therapy literature review of efficacy, cost effectiveness, and impact on patients' quality of life in chronic wound management and its implementation in the United kingdom. Plast Surg Int 2012:374398.

Padula WV, Delarmente BA (2019) The national cost of hospital-acquired pressure injuries in the United States. Int Wound J 16(3):634-640.

Paluch EK, Nelson CM, Biais N. et al (2015) Mechanotransduction: use the force(s). BMC Biol 13, 47.

Pandit V, Nesbitt SR, Kim DY, Mixon A, Kotha SP (2015) Combinatorial therapy using negative pressure and varying lithium dosage for accelerated wound healing. J Mech Behav Biomed Mater 44:173–8.

Pijuan J, Barceló C, Moreno DF, Maiques O, Sisó P, Marti RM, Macià A, Panosa A (2019) In vitro Cell Migration, Invasion, and Adhesion Assays: From Cell Imaging to Data Analysis. Front Cell Dev Biol 7:107.

Pinto BI, Cruz ND, Lujan OR, Propper CR, Kellar RS (2019) In Vitro Scratch Assay to Demonstrate Effects of Arsenic on Skin Cell Migration. J Vis Exp 23;(144).

Rajagopalan P, Marganski WA, Brown XQ, Wong JY (2004) Direct comparison of the spread area, contractility, and migration of balb/c 3T3 fibroblasts adhered to fibronectin- and RGD-modified substrata. Biophys J. 87(4):2818-2827.

Rodriguez-Menocal L, Salgado M, Ford D, Van Badiavas E (2012) Stimulation of skin and wound fibroblast migration by mesenchymal stem cells derived from normal donors and chronic wound patients. Stem Cells Transl Med 1(3):221–229.

Shkolyar A, Gefen A, Benayahu D, Greenspan H (2015) Automatic detection of cell divisions (mitosis) in live-imaging microscopy images using Convolutional Neural Networks. Conf Proc IEEE Eng Med Biol Soc. 2015:743-746.

Shoham N, Gottlieb R, Sharabani-Yosef O, Zaretsky U, Benayahu D, Gefen A (2012) Static mechanical stretching accelerates lipid production in 3T3-L1 adipocytes by activating the MEK signaling pathway. Am J Physiol Cell Physiol 15;302(2):C429-41.

Singer AJ, Clark RA (1999) Cutaneous wound healing. N Engl J Med 2;341(10):738-46.

Slomka N, Gefen A (2012) Relationship between strain levels and permeability of the plasma membrane in statically stretched myoblasts. Ann Biomed Eng 40, 606–618.

Stroncek JD, Reichert WM (2008) Overview of wound healing in different tissue types. In: Reichert WM, editor. Indwelling Neural Implants: Strategies for Contending with the In Vivo Environment. Boca Raton (FL): CRC Press/Taylor & Francis; Chapter 1.

Tai G, Tai M, Zhao M (2018) Electrically stimulated cell migration and its contribution to wound healing. Burns Trauma. 6:20.

Tokuyama E, Nagai Y, Takahashi K, Kimata Y, Naruse K (2015) Mechanical stretch on human skin equivalents increases the epidermal thickness and develops the basement membrane. PLoS One 10:e0141989.

Topman G, Sharabani-Yosef O, Gefen A (2011) A method for quick, low-cost automated confluency measurements. Microsc Microanal. 17(6):915-922.

Topman G, Sharabani-Yosef O, Gefen A (2012a) A standardized objective method for continuously measuring the kinematics of cultures covering a mechanically damaged site. Med Eng Phys 34(2):225-32.

Topman G, Lin FH, Gefen A (2012b) The influence of ischemic factors on the migration rates of cell types involved in cutaneous and subcutaneous pressure ulcers. Ann Biomed Eng. 40(9):1929-1939.

Topman G, Lin FH, Gefen A (2013a) The natural medications for wound healing - Curcumin, Aloe-Vera and Ginger - do not induce a significant effect on the migration kinematics of cultured fibroblasts. J Biomech 4;46(1):170-4.

Topman G, Shoham N, Sharabani-Yosef O, Lin FH, Gefen A (2013b) A new technique for studying directional cell migration in a hydrogel-based three-dimensional matrix for tissue engineering model systems. Micron 51:9-12.

Toume S, Gefen A, Weihs D (2016) Printable low-cost, sustained and dynamic cell stretching apparatus. J Biomech. 49(8):1336-1339.

Toume S, Gefen A, Weihs D (2017) Low-level stretching accelerates cell migration into a gap. Int Wound J 14(4):698-703.

Trepat X, Chen Z, Jacobson K (2012) Cell migration. Compr Physiol 2(4):2369-2392.

Undyala VV, DemboM, Cembrola K, Perrin BJ, Huttenlocher A, Elce JS, Greer PA, Wang YL, Beningo KA (2008) The calpain small subunit regulates cell-substrate mechanical interactions during fibroblast migration. J Cell Sci 121(pt 21):3581–8.

van Helvert S, Storm C, Friedl P (2018) Mechanoreciprocity in cell migration. Nat Cell Biol 20(1):8–20.

Vikatmaa P, Juutilainen V, Kuukasjärvi P, Malmivaara A (2008) Negative pressure wound therapy: a systematic review on effectiveness and safety Eur J Vasc Endovasc Surg 36, pp. 438-448.

Walter MN, Wright KT, Fuller HR, MacNeil S, Johnson WE (2010) Mesenchymal stem cell-conditioned medium accelerates skin wound healing: an in vitro study of fibroblast and keratinocyte scratch assays. Exp Cell Res 316(7):1271-81.

Wiegand C, White R. Microdeformation in wound healing (2013) Wound Repair Regen 21(6):793-9.

Yadav S, Rawal G, Baxi M. Vacuum assisted closure technique: a short review (2017) Pan Afr Med J 28:246.

Figure captions

Figure 1	The miniature incubator for cell stretching (MICS): (a) The dynamic stretching device (a photo of the system is shown on the left-hand side and a drawing is on the right), (b) a cross-sectional view of one culture well in the dynamic stretching device and (c) the incubation chamber occupying the dynamic stretching device, the tent structure is not shown.
Figure 2	A curve fit of mean Euleriam strains (*E*) versus plate displacement (*d*) measured in the calibration experiments conducted for the dynamic cell stretching device
Figure 3	Experimental design: (a) the custom 3D-printed cross handle used for creation of the 'wound' gap in a 3D view with the needle inside located on a Flexcell (BioFlex®, International Corporations, Burlington, NC, USA) culture plate. (b) The five different 'wound' assay stretching protocols that were applied.
Figure 4	An example of gap area versus time plots for each of the five different stretching protocols: (a) static stretch, including several corresponding frames of the temporal assay data which demonstrate the spatial gap closure pattern. (b) No stretch. (c) Cyclic stretching at a frequency of 0.1 Hz. (d) A '2-5' stretching protocol (defined in the text). (e) Cyclic stretching at a frequency of 1 Hz.
Figure 5	Kinematics of the gap closure by fibroblasts for the different stretch protocols studied here where the peak stretch level was set to 3% (left column) or 0.5% (right column). The normalized maximum migration rates for these peak stretch levels are shown in panels (a) and (b), respectively. The times for closure of 90% of the initial gap area for the aforementioned two stretch levels are depicted in panels (c) and (d), respectively. Asterisks mark statistically significant results ($p<0.05$).

Declarations: The authors have no conflicts of interest to declare.

Funding: This research work was partially supported by the Israel Science Foundation grant no. 1266/16 and by the European Union's Horizon 2020 research and innovation programme under the Marie Skłodowska-Curie grant agreement no. 811965.

Conflicts of interest/Competing interests: The authors declare that they have no conflict of interest.

Ethics approval: Not applicable.

Consent to participate: Not applicable.

Consent for publication: Provided by all authors.

Availability of data and materials: The data and materials are available.

Code availability: The Matlab code used for the present analyses is available.

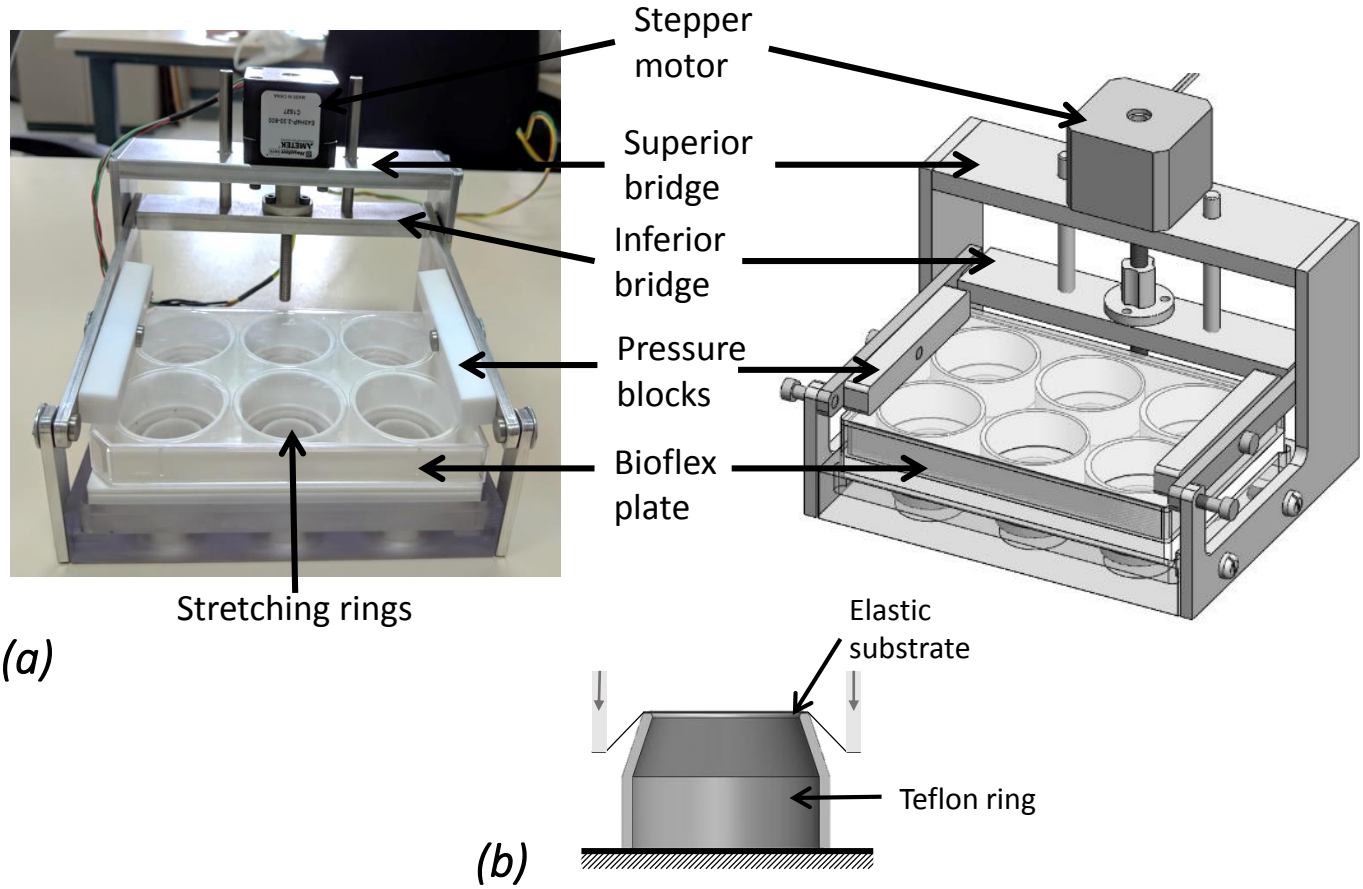
Stepper motor
Superior bridge
Inferior bridge
Pressure blocks
Bioflex plate
Stretching rings
(a)
Elastic substrate
Teflon ring
(b)

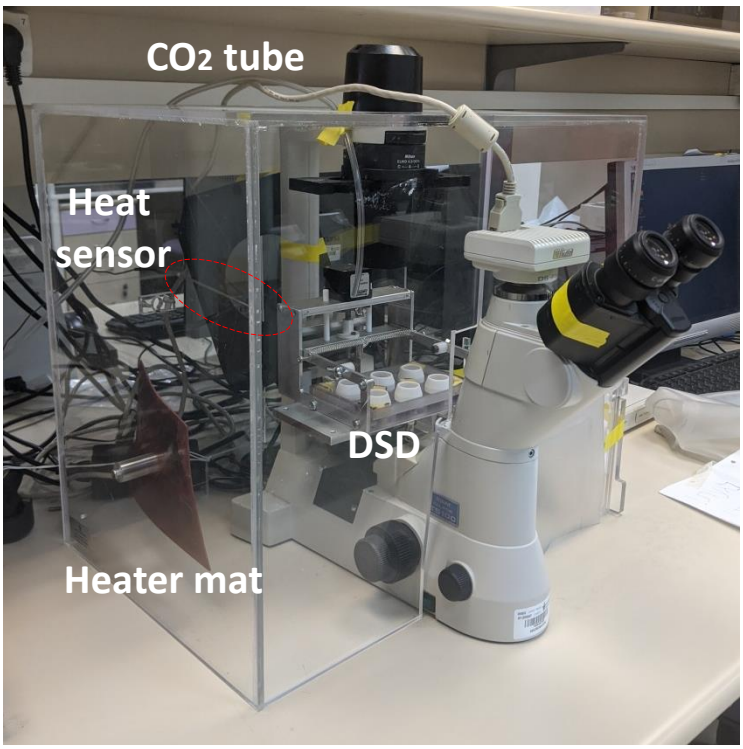
CO2 tube
Heat sensor
DSD
Heater mat
(c)

Figure 1

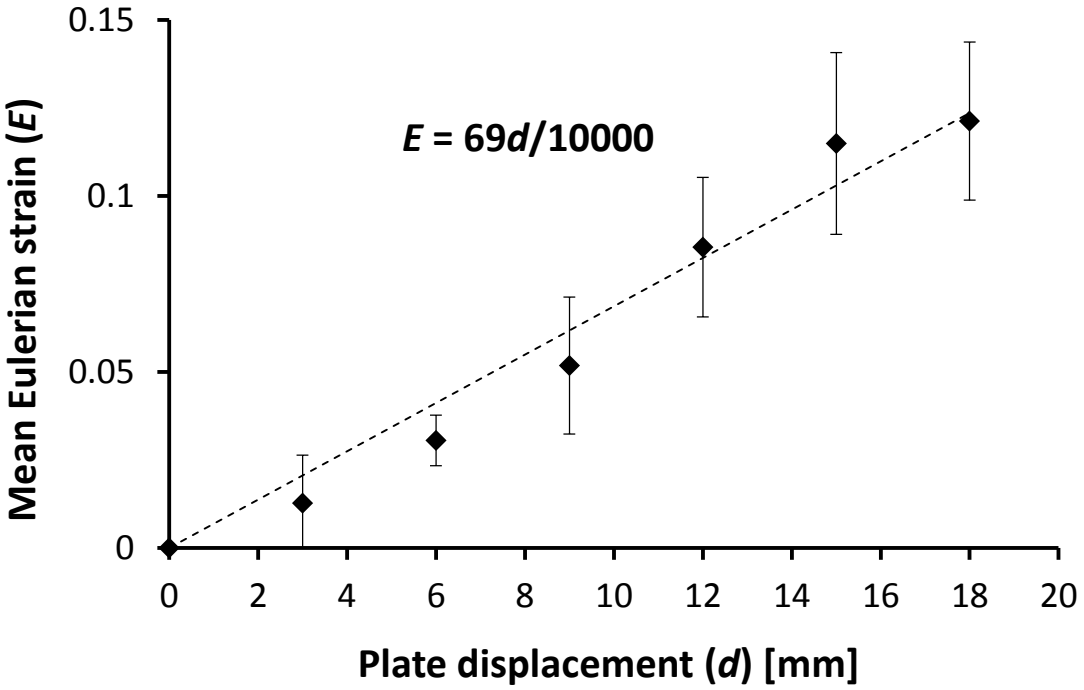
0.15
0.1
0.05
0
Mean Eulerian strain (E)
E = 69d/10000
0
2
4
6
8
10
12
14
16
18
20
Plate displacement (d) [mm]

Figure 2

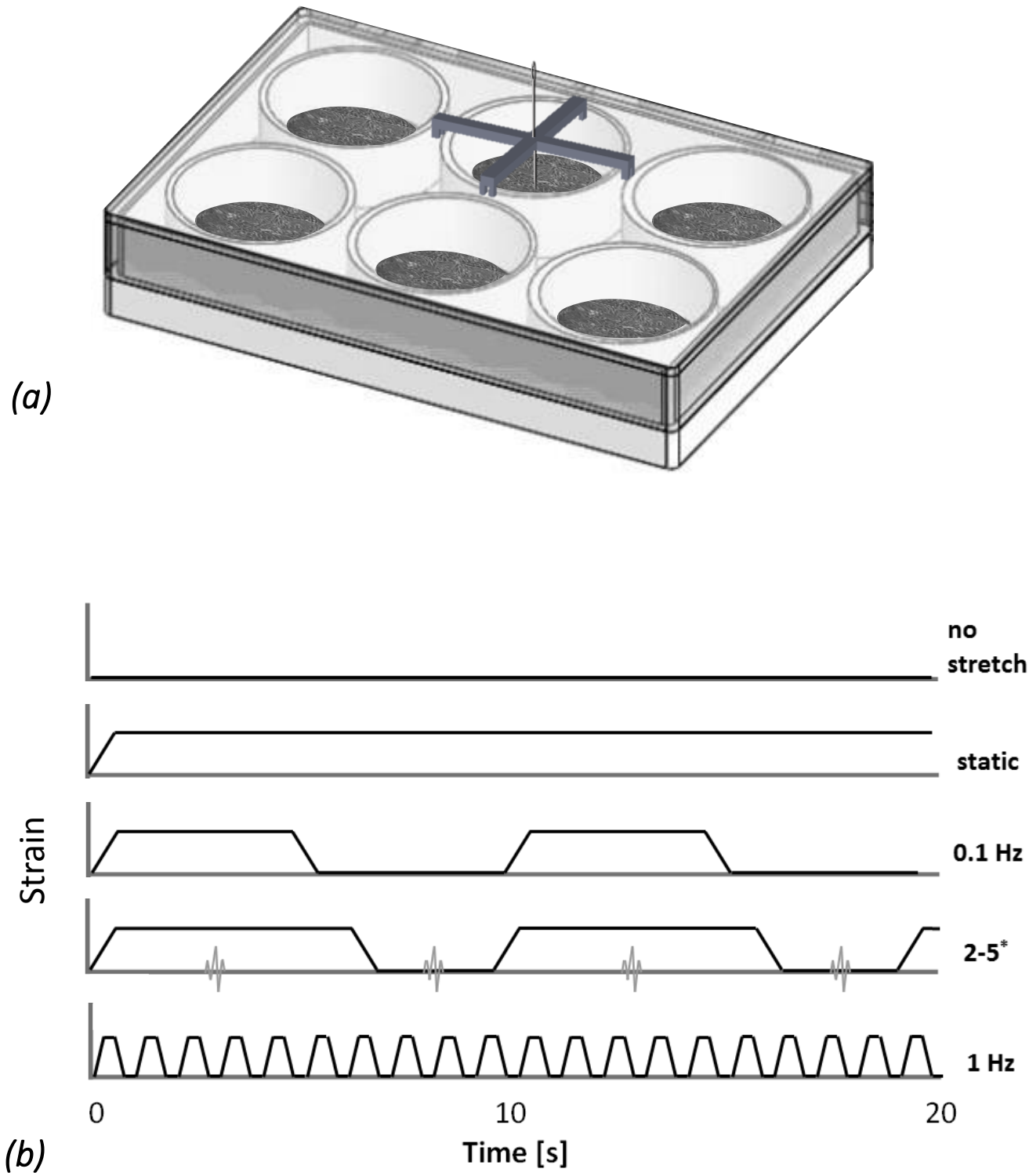

Figure 3

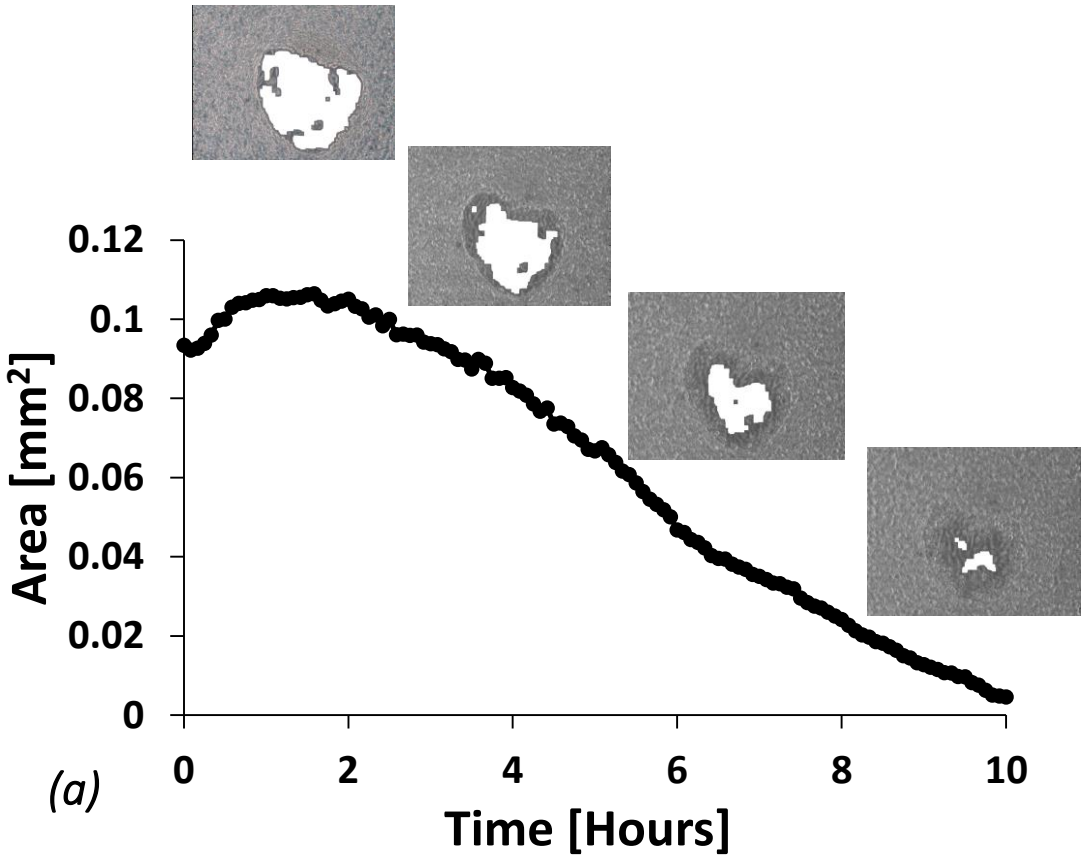
0.12
0.1
0.08
0.06
0.04
0.02
0
Area [mm²]
0
2
4
6
8
10
Time [Hours]
(a)

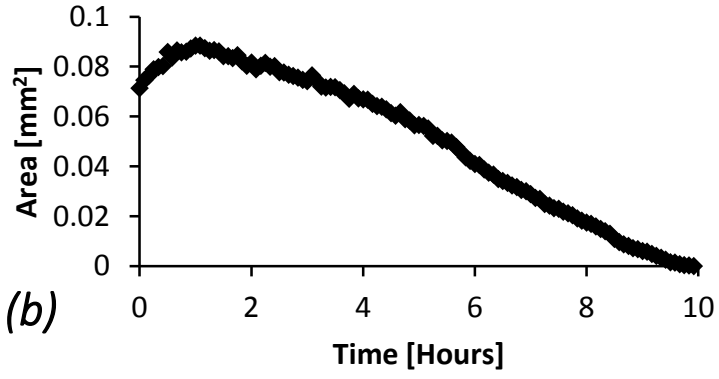
0.1
0.08
0.06
0.04
0.02
0
Area [mm²]
0
2
4
6
8
10
Time [Hours]
(b)

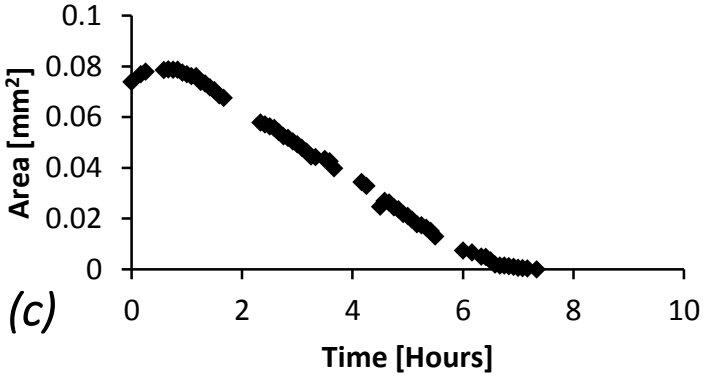
0.1
0.08
0.06
0.04
0.02
0
Area [mm²]
0
2
4
6
8
10
Time [Hours]
(c)

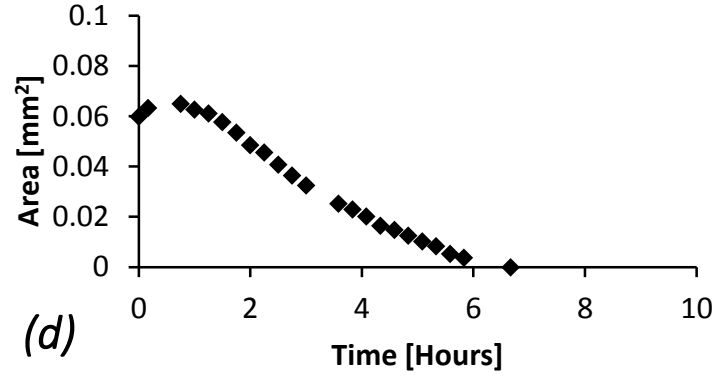
0.1
0.08
0.06
0.04
0.02
0
Area [mm²]
0
2
4
6
8
10
Time [Hours]
(d)

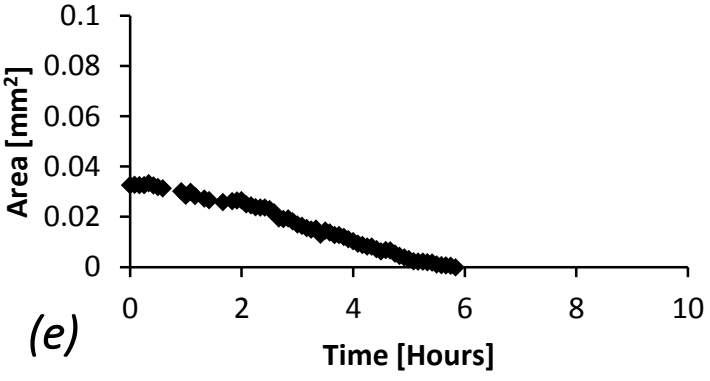
0.1
0.08
0.06
0.04
0.02
0
Area [mm²]
0
2
4
6
8
10
Time [Hours]
(e)

Figure 4

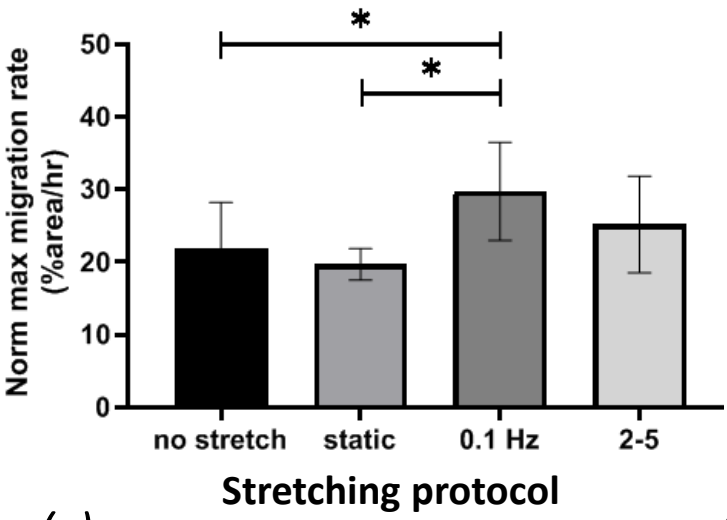

(a)

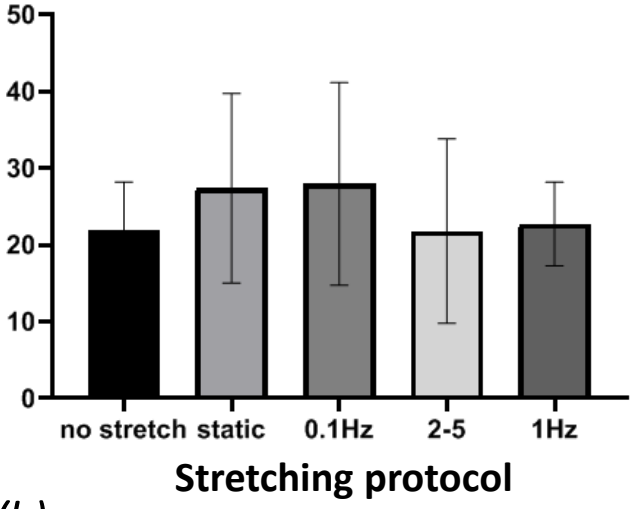

(b)

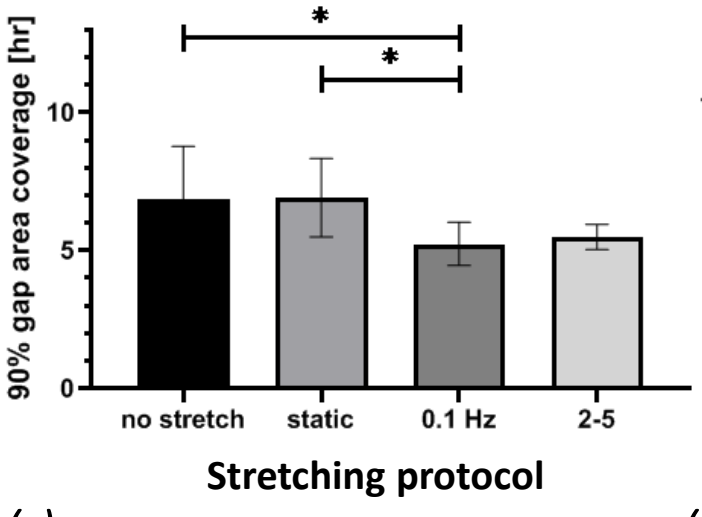

(c)

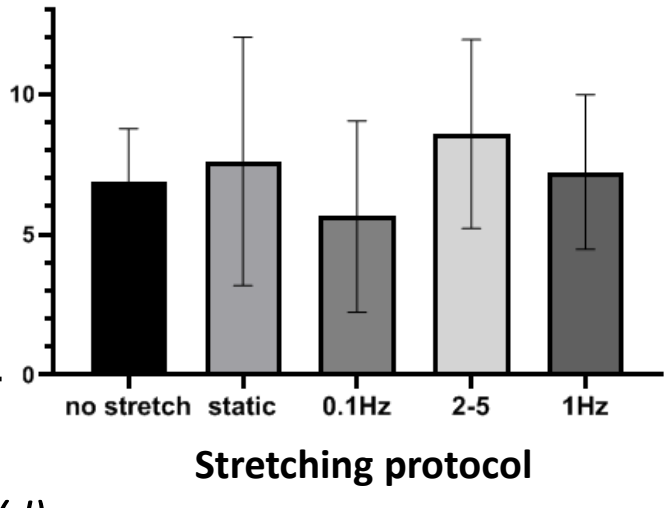

(d)

Figure 5